**EPJ manuscript No.**
(will be inserted by the editor)

# Measurement of $D^0$, $D^+$, $D_s^+$ and $D^{*+}$ Production in Fixed Target 920 GeV Proton-Nucleus Collisions

HERA-B Collaboration

HERA-B Institutions

Received: date / Revised version: date

**Abstract.** The inclusive production cross sections of the charmed mesons $D^0, D^+, D_s^+$ and $D^{*+}$ have been measured in interactions of 920 GeV protons on C, Ti, and W targets with the HERA-B detector at the HERA storage ring. Differential cross sections as a function of transverse momentum and $x_{\mathrm{F}}$ are given for the central rapidity region and for transverse momenta up to $p_{\mathrm{T}} = 3.5$ GeV/$c$. The atomic number dependence and the leading to non-leading particle production asymmetries were measured as well.
Version 5.1, July 16, 2007

**PACS.** 13.85.Ni Inclusive production with identified hadrons – 24.85.+p Quarks, gluons, and QCD in nuclei and nuclear processes – 13.20.Fc Decays of charmed mesons

## 1 Introduction

The cross sections for charm and beauty hadroproduction are of considerable theoretical interest [1]. Perturbative QCD is expected to work well for the large mass top quark production and less well for the lower mass $b$ and $c$ quarks [1–3]. At present, there exist several published results on measurements of charm production in proton-nucleus collisions [4]-[9]. They are mainly restricted to beam energies between 200 GeV and 800 GeV, and mostly have low statistics. Only one of the experiments also provides a measurement of the atomic number dependence. More data could help in determining the strong interaction parameters as well as guiding the calculation of non-perturbative effects. Another motivation comes from the recent observation that the ratio of open charm to charmonium cross sections in $pA$ reactions is essential for quark-gluon plasma searches [10]. The present work provides a new data point at 920 GeV proton beam energy.

Collisions of the 920 GeV HERA proton beam in C, Ti and W fixed targets have been measured with the HERA-B spectrometer. In previous papers we have reported on the $b\bar{b}$ [11], $\Upsilon$ [12], and charmonium [13,14] production cross sections, while the present work deals with production of open charm in the inclusive reactions $pA \rightarrow DX$. Here $D$ represents a $D^0, D^+, D_s^+$ or $D^{*+}$ detected through the following decay channels: $D^0 \rightarrow K^-\pi^+$, $D^+ \rightarrow K^-\pi^+\pi^+$, $D_s^+ \rightarrow \phi\pi^+ \rightarrow K^-K^+\pi^+$, and $D^{*+} \rightarrow D^0\pi^+ \rightarrow K^-\pi^+\pi^+$. Throughout this paper, charge-conjugate modes are included unless noted otherwise.

The paper is organized as follows. We first briefly describe the apparatus, the data sample and the method of analysis. We then present the results and finally make a comparison with other measurements and theoretical expectations.

## 2 The detector

HERA-B was a fixed target spectrometer (see Fig. 1) using the 920 GeV proton beam of the HERA $e$-$p$ collider. Interactions occurred in two groups of 4 target wires with typical transverse dimensions between 50 $\mu$m and 500 $\mu$m, separated by 4 cm [15]. The wires were located in the beam halo, and their distance to the beam core was automatically adjusted to maintain a constant interaction rate. Details of the various subdetectors have been published [16]-[22], so only a brief overview of the apparatus is given here.

Tracks from proton interactions and decay vertices were measured with a vertex detector system (VDS) [16]. Sixty-four silicon strip detectors with double-sided readout ($50\times 70$ mm$^2$, pitch of $\sim$50 $\mu$m) were arranged in eight stations between 7 cm and 200 cm downstream of the targets. The detectors were in Roman pots [23] under vacuum and their inner edges were adjusted to be in the range 10-15 mm from the beam center. With this system a vertex resolution of $\sigma_z \sim 500$ $\mu$m along the beam direction and $\sigma_{x,y} \sim 50$ $\mu$m in the transverse plane was achieved.

Particle momenta were measured with a tracking system and a dipole magnet of 2.13 T-m field integral. The first tracking chamber was in front of the magnet, and the remaining six chambers were behind the magnet between 7 m and 13 m downstream of the interaction region. Due to large differences in particle flux density, the tracking system was divided into a fine grained inner tracker

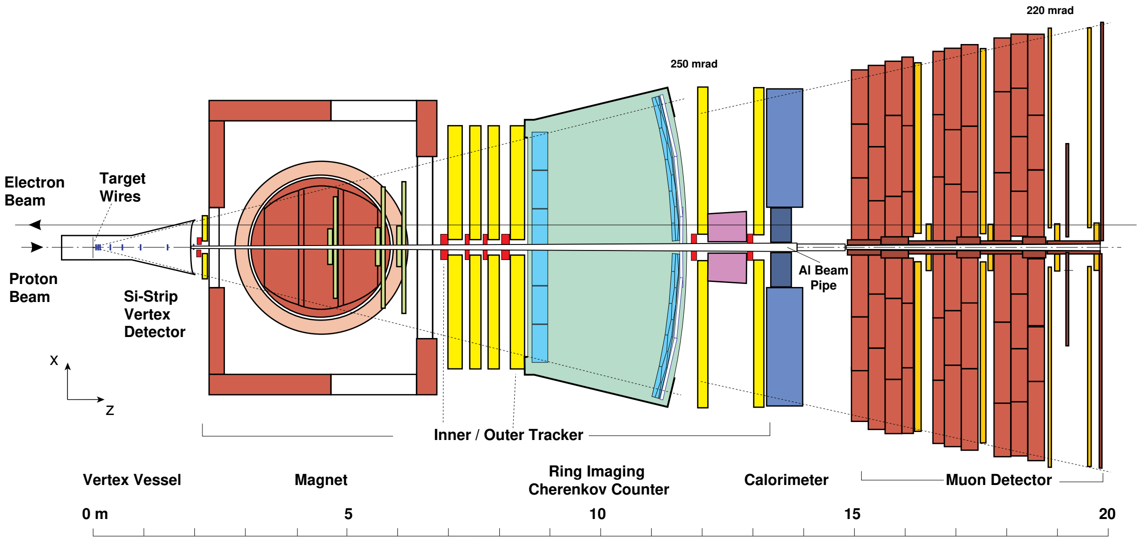


**Fig. 1.** A top view of the HERA-B detector.

(ITR – microstrip gas chambers with gas electron multipliers and typically 300 $\mu$m pitch [17]) and a coarse grained outer tracker (OTR – honeycomb drift cells with 5 mm and 10 mm cell diameters [18]). The momentum resolution can be parametrized as $\sigma_p/p = (1.61 + 0.0051pc/\mathrm{GeV})\%$ [19], where $p$ is the particle momentum.

Particle identification was achieved with three subdetectors: a ring imaging Cherenkov counter (RICH), an electromagnetic calorimeter (ECAL) and muon chambers (MUON). The RICH detector [20] is a large vessel containing about 100 m$^3$ of $C_4F_{10}$ gas at STP, which provided about 2 m of radiation path. The Cherenkov photons were focused and reflected by two sets of spherical and planar mirrors onto an upper and a lower photon detector. Each photon detector consisted of about 1100 multi-anode photomultiplier tubes. The pion efficiency was about 90% in the momentum range slightly above the pion threshold (2.4 GeV/$c$) up to 70 GeV/$c$ with a kaon misidentification probability below 10%, while the kaon efficiencies were above 85% for kaon momenta between 15 GeV/$c$ and 45 GeV/$c$ with a pion misidentification of $\sim$1%. For kaons below the Cherenkov threshold of $\sim$10 GeV/$c$, the misidentification of pions was kept below 10%.

The ECAL [21] was a sampling calorimeter of the "shashlik" type, with scintillator plates sandwiched between tungsten (inner region) or lead (outer region) absorbers and read out by optical fibers and photomultiplier tubes. The readout granularity of inner and outer regions was also adapted to different particle rates in order to maintain acceptable occupancies. The MUON system [22], situated in the most downstream region, consisted of four large detector stations separated by iron absorbers. Each muon detector plane had gas pixel chambers in the inner region and gas proportional tubes in the outer region.

For the present measurement, the analysis of data was based on the following components: the vertex detector (VDS), the OTR tracking system and the RICH counter.

**Table 1.** Summary of the data statistics and the integrated luminosities of the present study.

| Target | A | events [$\times 10^6$] | $\mathcal{L}$ [$\mu b^{-1}$] |
|---|---|---|---|
| C | 12.01 | 89.3 | 375 |
| Ti | 47.88 | 24.7 | 31 |
| W | 183.84 | 67.6 | 36 |

## 3 Data analysis

The study was performed on data sets with a single target wire made either of carbon, titanium or tungsten. Only runs with stable conditions and a minimum bias trigger with a total of 182 million interactions (Table 1) were considered. The trigger required at least 20 hits in the RICH detector (compared to an average of 33 for a full ring from a $\beta = 1$ particle [20]) and had an efficiency $\epsilon_{\mathrm{trigger}} \approx 95\%$ for inelastic interactions with the total inelastic cross section $\sigma_{\mathrm{inel}}$. The integrated luminosity $\mathcal{L}$ was determined [24] from the number of inelastic interactions $N_{\mathrm{inel}}$ using the expression $\mathcal{L} = N_{\mathrm{inel}}/(\epsilon_{\mathrm{trigger}}\sigma_{\mathrm{inel}})$. The data were recorded at a moderate interaction rate of about 1.5 MHz which corresponds to 0.17 interactions per filled bunch crossing. Therefore only about 10% of triggered events contain more than one interaction. The data acquisition rate was about 1 kHz, and the bulk of the data was recorded within a two-week minimum bias run.

At the HERA-B energy the charm production cross section is more than two orders of magnitude smaller than the inelastic cross section. Taking into account also the relatively small branching ratios for the $D$ meson decay modes into two or three charged particles in the final state, one finds sizeable backgrounds. Particle identification alone is not sufficient to extract signals. However, the large boost of the center-of-mass system of HERA-B ($\gamma = 22$), causing $D$ mesons to decay several millimeters from the target, combined with good vertex resolution

($\approx$0.5 mm) allows us to distinguish $D$ meson decay products from the particles originating at the primary interaction point. The data selection thus required a detached secondary vertex, formed by tracks not coming from the primary interaction point as well as the identification of kaons and pions. The selection criteria are summarized in Table 2 and discussed in some detail below.

### 3.1 Data selection

Since a detached vertex is required for the ground state $D$ mesons, only events with at least one reconstructed primary vertex were selected. Primary vertices were determined from all track segments reconstructed in the VDS. Since the proton interaction point is inside the target wire, the measured primary vertex position in the coordinates transverse to the wire orientation was replaced with the known target wire position.

For the tracks corresponding to the decay products of $D$ mesons, mild requirements were applied on the number of hits in the vertex detector and the main tracking system, and on the track fit quality. The following selection criteria based on information from the RICH counter were used to identify the final state kaons and pions: while a rather strict cut on the kaon likelihood[1] was required for the kaon candidates ($L_K > 0.5$ for the $D^0$ and $D^+$ selection, and $L_K > 0.33$ for $D_s^+$ candidates), for pions only a mild cut $L_e + L_\mu + L_\pi > 0.05$ was applied on the sum of RICH likelihoods for electrons, muons and pions. No particle identification requirement was imposed for pions from $D^{*+} \to D^0\pi^+$ decays, which tend to have low momenta and thus are denoted as $\pi_{\rm slow}$.

The tracks were combined to form $D^0, D^+$ and $D_s^+$ candidates. Candidates with an invariant mass in the interval of $\pm$500 MeV around the $D$ meson nominal mass were retained for further analysis. For the $D_s^+$ candidates, two additional cuts were applied. The invariant mass of the $K^+K^-$ pairs was required to be in the interval of $\pm$10 MeV around the $\phi$ nominal mass; the absolute value of the cosine of the angle $\theta_\phi$ between the $K^+$ and $\pi$ in the rest frame of the $\phi$ was restricted to the values above 0.5, exploiting the vector nature of the intermediate state $\phi$. The $D^{*+}$ candidates were reconstructed from $D^0$ candidates with invariant mass $\pm$75 MeV around the $D^0$ mass and slow pion candidates, after a vertex fit to $D^0$. For the $D^{*+}$ candidates, an additional cut was applied on the product of transverse momenta of the $D^0$ daughter tracks and of the $D^0$ momentum, $\zeta = p(D^0)p_{\rm T}(K)p_{\rm T}(\pi)$.

In addition to the cuts described above, the analysis was restricted to the region of phase space with a high acceptance, $-0.15 < x_{\rm F} < 0.05$. A common vertex for each track combination was fitted. Only combinations with a probability greater than 0.1% and with a secondary vertex displaced by more than 4 standard deviations downstream of the wire were accepted.

[1] Likelihoods for the electron, muon, pion, kaon, proton and background hypotheses are normalized such that their sum is equal to 1, $L_e + L_\mu + L_\pi + L_K + L_p + L_{\rm bkg} = 1$.

The $D$ meson candidate was then associated with the primary vertex. In the case of events with multiple reconstructed primary vertices, the vertex with the smallest impact parameter significance (i.e., the measured value divided by its estimated error given by the covariance matrix) with respect to the track of the $D$ meson candidate was chosen. To avoid possible bias in the primary vertex position due to tracks from the $D$ meson candidate, the primary vertex was refitted without the $D$ daughter tracks.

The final set of criteria was based on the primary and secondary vertices. The main source of background, combinations of particles emerging from the primary interaction point, was reduced by the following requirements: (1) the secondary vertex is detached, (2) the tracks forming the secondary vertex do not come from the primary interaction point and (3) the $D$ meson candidate originates from the primary interaction point. To fulfill these criteria, cuts were applied on the following variables:

- $d(D)$ the distance significance of the secondary vertex to the associated primary vertex,
- $b(\pi), b(K)$ the impact parameter significance of a pion or a kaon to the primary vertex (in case more than one primary vertex was found, that closest to the particle is chosen),
- $b(D)$ the impact parameter significance of a $D$ meson candidate with respect to the associated primary vertex.

We found that for the three-body decays of $D^+$ and $D_s^+$, a more effective cut than a selection based on single impact parameter significances of daughter tracks is a cut on their product $b(K)b(\pi_1)b(\pi_2)$ and $b(K_1)b(K_2)b(\pi)$, respectively.

By studying the correlation between the cut on the product of impact parameter significances and the proper lifetime, it was found that the signal significance, the ratio $S/\sqrt{S+B}$, with $S$ being the number of signal events and $B$ the number of background events, could be improved with criteria of the form $\sqrt[3]{b(K)b(\pi_1)b(\pi_2)} > 4(t - t_0)$, for $D^+$, and $\sqrt{b(\phi)b(\pi)} > 0.75(t - t_0)$, for $D_s^+$. Here the proper lifetime $t$ is in units of the $D$ mean lifetime, and the offset $t_0$ is determined in an optimization.

For each decay mode the optimal cuts were determined by maximizing the signal significance $S/\sqrt{S+B}$ in a $\pm3\sigma$ window centered at the $D$ meson nominal mass (signal window). The signal $S$ was taken from Monte Carlo simulation and was scaled to the luminosity of real data by using an estimation for the production cross sections from fits to the published $D$ meson cross sections [1]. For the $D_s^+$ the cross section was assumed to amount to 20% of the sum of the $D^0$ and $D^+$ cross sections [2].

In the case of ground state $D$ mesons, the number of background events $B$ was estimated from the data sidebands. For the $D_s^+$, the mass region of $\pm$50 MeV around the nominal mass of the $D^+$, where a contribution of the decay $D^+ \to \phi\pi^+$ is expected, was excluded from the lower sideband. To reduce the sensitivity to statistical fluctuations, the sidebands were chosen to be larger than the signal window. In the case of the $D^{*+}$, the wrong sign combinations from real data were used to estimate the background in the signal window. As is usually done for this decay, the signal was reconstructed via the mass difference $q = m(K, \pi, \pi_{\rm slow}) - m(K, \pi) - m_\pi$ rather than using the invariant mass of the $K, \pi, \pi_{\rm slow}$ combinations.

After applying the selection cuts, which are summarized in Table 2, the remaining data were scanned for events with more than one $D$ meson candidate. In case of the $D^0$, $D^+$ and $D_s^+$ candidates, the candidate with the largest decay distance significance $d(D)$ was kept. For the $D^{*+}$ analysis, first the candidates were selected where the intermediate $D^0$ had the largest decay distance significance. If multiple candidates remained (i.e., due to multiple $\pi_{\rm slow}$ candidates), the $D^{*+}$ candidate with the highest vertex probability was kept.

### 3.2 Signal yields

The invariant mass distributions for $D$ meson candidates after applying the selection criteria discussed above are shown in Figs. 2-4.

The signal yield was extracted from the histograms by a maximum likelihood fit assuming Poissonian statistics in individual bins. A Gaussian function was used for the signal, while the background description depended on the type of the $D$ meson. For the $D^+$ and $D_s^+$, the background was fitted by an exponential function. The background for $D^0$ candidates is more complicated and consists of a combinatorial part, fitted by an exponential, and a contribution from partially reconstructed charm decays. This latter background is visible in the mass range below the $D^0$ peak. The shape of this background is taken from Monte Carlo simulation of $c\bar{c}$ events to which selection criteria had been applied.

In the $D_s^+$ invariant mass distribution the Cabibbo suppressed decay of $D^+ \to \phi\pi^+$ is also seen (the peak to the left of the $D_s^+$ peak). This peak is included in the fit function as an additional Gaussian of the same width as the signal Gaussian, with its normalization as an additional free parameter, and its mean fixed to that extracted from the $D^+ \to K^-\pi^+\pi^+$ invariant mass distribution. The background for the $D^{*+}$ candidates was parameterized as $a(q^{1/2} + bq^{3/2})$, with $a$ and $b$ as free parameters.

The fitted peak positions are within one standard deviation of the corresponding PDG values [25], with the exception of $D_s^+$, which deviates by less than two standard deviations. The widths of the signal peaks are about 30% larger than the corresponding Monte Carlo values.

The numbers of reconstructed $D$ mesons are summarized in Table 3. In total, 175 $D^0$, 131 $D^+$, 11 $D_s^+$ and 61 $D^{*+}$ decays were reconstructed. The yields for various subsamples (particle, anti-particle, individual target material) were obtained by fixing the mean and $\sigma$ of the signal Gaussian function to the values obtained from the fit to the full sample.

To check the signal consistency, the $D$ meson proper time distributions were measured. The acceptance-corrected distributions were confirmed to be exponential. To determine the lifetimes, a simultaneous likelihood fit of

**Table 2.** Selection criteria; the definitions of variables are given in the text.

| |
|---|
| $D^0 \to K^-\pi^+$ |
| chosen a priori |
| $L_K(K) > 0.5$<br>$L_e(\pi) + L_\mu(\pi) + L_\pi(\pi) > 0.05$ |
| optimized using background data and signal MC |
| $d(D^0) > 6.1$<br>$b(D^0) < 2.4$<br>$b(K) > 3.4$<br>$b(\pi) > 3.7$ |
| $D^+ \to K^-\pi^+\pi^+$ |
| chosen a priori |
| $L_K(K) > 0.5$<br>$L_e(\pi) + L_\mu(\pi) + L_\pi(\pi) > 0.05$ |
| optimized using background data and signal MC |
| $b(D^+) < 2.6$<br>$b(K)b(\pi_1)b(\pi_2) > 106$<br>$\sqrt[3]{b(K)b(\pi_1)b(\pi_2)} > 4(t - t_0),\ t_0 = 2.48$ |
| $D_s^+ \to \phi\pi^+ \to K^-K^+\pi^+$ |
| chosen a priori |
| $L_K(K) > 0.33$<br>$L_e(\pi) + L_\mu(\pi) + L_\pi(\pi) > 0.05$<br>$\lvert m(K^+K^-) - m(\phi)\rvert < 10$ MeV<br>$\lvert\cos(\theta_\phi)\rvert > 0.5$ |
| optimized using background data and signal MC |
| $d(D_s^+) > 5.3$<br>$b(D_s^+) < 2.11$<br>$b(K^-)b(K^+)b(\pi) > 28.7$<br>$\sqrt{b(\phi)b(\pi)} > 0.75(t - t_0),\ t_0 = 1.0$ |
| $D^{*+} \to D^0\pi^+ \to K^-\pi^+\pi^+$ |
| chosen a priori |
| $L_K(K) > 0.5$<br>$L_e(\pi) + L_\mu(\pi) + L_\pi(\pi) > 0.05$<br>$\lvert m(K\pi) - m(D^0)\rvert < 75$ MeV<br>$d(D^0) > 4$ |
| optimized using background data and signal MC |
| $b(D^0) < 2.4$<br>$b(K) > 2.1$<br>$b(\pi) > 1.7$<br>$\zeta(D^0) > 17.7($ GeV/c$)^3$ |

**Table 3.** Number of reconstructed $D$ mesons.

| sample | $D^0$ | $D^+$ |
|---|---|---|
| total | 174.8±16.8 | 130.5±14.7 |
| particle | 75.9±10.9 | 54.5±9.3 |
| anti-particle | 99.0±11.9 | 75.8±10.5 |
| C | 66.1±9.6 | 43.1±7.7 |
| W | 92.3±11.7 | 72.4±10.6 |
| Ti | 17.4±5.7 | 14.9±5.0 |

| sample | $D_s^+$ | $D^{*+}$ |
|---|---|---|
| total | 11.4±4.0 | 61.3±13.0 |
| particle | 4.9±2.6 | 21.0±6.6 |
| anti-particle | 6.7±2.8 | 40.6±8.3 |
| C | 4.2±2.2 | 26.6±6.4 |
| W | 6.7±3.0 | 24.8±7.5 |
| Ti | 0.4±1.0 | 9.6±4.0 |

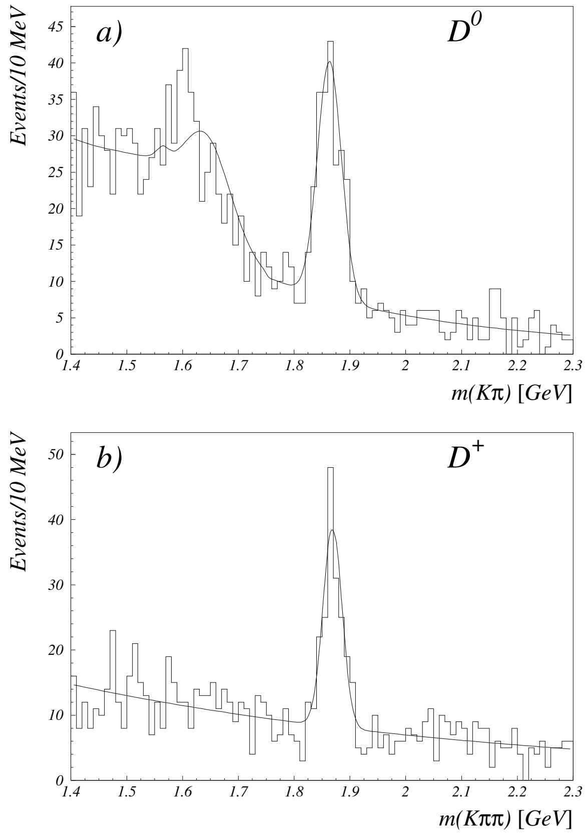


**Fig. 2.** Invariant mass distributions for $K^-\pi^+$ (a) and $K^-\pi^+\pi^+$ (b) combinations.

events in the signal window and in the sidebands was used. The results, $c\tau = (302 \pm 33)$ $\mu$m for $D^+$, $(120 \pm 13)$ $\mu$m for $D^0$, and $(165 \pm 52)$ $\mu$m for $D_s^+$, are in good agreement with the PDG values [25].

As a further consistency check of the $D_s^+$ and $D^{*+}$ signals, the intermediate states $\phi$ and $D^0$ were checked. They should be visible in the corresponding invariant mass distributions, when the signal region in the initial state in-

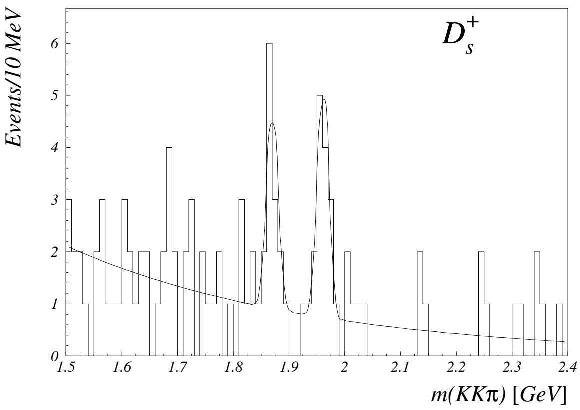


**Fig. 3.** Invariant mass distributions for $\phi\pi^+ \to (K^-K^+)\pi^+$ combinations. Besides the $D_s^+$ peak at 1.96 GeV also the $D^+$ peak at 1.87 GeV is seen, corresponding to the Cabibbo suppressed decay $D^+ \to \phi\pi^+$.

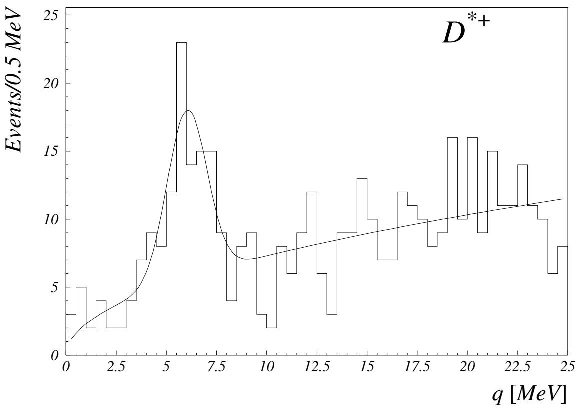


**Fig. 4.** Invariant mass difference $q = m(K, \pi, \pi_{\rm slow}) - m(K, \pi) - m_\pi$ for $K^-\pi^+\pi^+$ combinations.

variant mass distribution is selected, and the fit to the intermediate state invariant mass distribution should give the number of events consistent with the number in the initial state peak. The yields extracted in this way are in good agreement with the values given in Table 3. For the $D_s^+$ decays, the distribution of the cosine of the angle between $K^+$ and $\pi$ in the rest frame of the $\phi$ was found to be consistent with the expectation given by the vector nature of the intermediate state $\phi$. The $D^+ \to \phi\pi^+$ signal yield was checked by estimating the number of reconstructed decays from our measured $D^+$ cross section in the $D^+ \to K^-\pi^+\pi^+$ decay channel. The fitted number of events, 9.8±3.8, is in reasonable agreement with the estimated number (4.2±1.2).

## 4 Efficiency determination

A Monte Carlo simulation is used to determine the signal reconstruction efficiencies. The Monte Carlo samples for $pA \to DX$ are generated in two steps. First, a $c\bar{c}$ pair is generated with Pythia 5.7 [26] such that a particular

$D$ meson is always produced. The generated events are reweighted to make the resulting cross sections conform to the parameterizations

$$\frac{d\sigma}{dp_{\mathrm{T}}^2} \propto \left[1+\left(\frac{\sqrt{\pi}\,\Gamma(\beta-\frac{3}{2})\,p_{\mathrm{T}}}{2\,\Gamma(\beta-1)\,\langle p_{\mathrm{T}}\rangle}\right)^2\right]^{-\beta} \tag{1}$$

and

$$\frac{d\sigma}{dx_{\mathrm{F}}} = \begin{cases} A\exp\left(-\frac{x_{\mathrm{F}}^2}{2\sigma_g^2}\right) &, |x_{\mathrm{F}}| < x_{\mathrm{b}} \\ A'\left(1-|x_{\mathrm{F}}|\right)^n &, |x_{\mathrm{F}}| \geq x_{\mathrm{b}} \end{cases} \tag{2}$$

with $\sigma_g = \sqrt{\frac{x_{\mathrm{b}}(1-x_{\mathrm{b}})}{n}}$ and $\ln\frac{A}{A'} = n[\frac{x_{\mathrm{b}}}{2(1-x_{\mathrm{b}})} + \ln(1-x_{\mathrm{b}})]$ [27]. The average transverse momentum of $\langle p_{\mathrm{T}}\rangle = 1.04 \pm 0.04$ GeV/$c$ and the value of the exponent $\beta = 7.0 \pm 4.3$ are taken from the present analysis (Sec. 5.2). The value $n = 7.7 \pm 1.4$ was taken from the average of E743 and E653 [6,7], and $x_{\mathrm{b}}$ was assumed to be The influence of the parameter uncertainties and other possible parametrisations of expression Eq. 2 are taken into account as systematic errors. After the generation of the $D$ mesons, the remaining energy is input to the Fritiof 7.02 [28] program package which generates the underlying event taking into account further interactions inside the nucleus.

The detector response is simulated with the Geant 3.21 package [29]. Realistic detector efficiencies, readout noise and dead channels are taken into account. The simulated events are processed by the same reconstruction codes as that used for the data.

## 5 Results

### 5.1 Total cross sections

The visible cross section per nucleus, i.e., the cross section measured in our visible range of $-0.15 < x_{\mathrm{F}} < 0.05$, is given by

$$\Delta\sigma_{\mathrm{pA}} = \frac{N_i}{\mathrm{Br}\cdot\epsilon_i\cdot\mathcal{L}_i}, \tag{3}$$

where $N_i$ is the number of reconstructed $D$ mesons for a particular target, $\epsilon_i$ and $\mathcal{L}_i$ are the corresponding efficiency and integrated luminosity, and Br is the branching ratio for a specific decay channel [25]. The cross section for $D$ meson production on a nuclear target of atomic number $A$ is parameterized as

$$\sigma_{\mathrm{pA}} = \sigma_{\mathrm{pN}}\cdot A^{\alpha}. \tag{4}$$

To combine data recorded with different target materials, the production cross sections per nucleon $\Delta\sigma_{\mathrm{pN}}$ were extracted in the following way. From equations Eq. 3 and Eq. 4, the $D$ meson yield of the target $i$ is derived,

$$N_i = \mathrm{Br}\cdot\epsilon_i\cdot\mathcal{L}_i\cdot\Delta\sigma_{\mathrm{pN}}\cdot A_i^{\alpha} \tag{5}$$

**Table 4.** Summary of systematic uncertainties of reconstruction efficiency.

| Source | $D^0$ | $D^+$ | $D_s^+$ | $D^{*+}$ |
|---|---|---|---|---|
| Monte Carlo statistics | 1.2% | 1.3% | 3.7% | 1.1% |
| Track reconstruction | 3.0% | 4.5% | 4.5% | 4.5% |
| Particle identification | 4.0% | 6.0% | 6.0% | 4.0% |
| Selection criteria | 6.0% | 6.0% | 6.0% | 6.0% |
| Re-weighting | 2.9% | 3.6% | 7.7% | 4.6% |
| Total | 8.4% | 10.3% | 12.9% | 9.7% |

By summing Eq. 5 over all targets and solving it for the production cross section we get

$$\Delta\sigma_{\mathrm{pN}} = \frac{N}{\mathrm{Br}\cdot\sum_i \epsilon_i\mathcal{L}_i A_i^{\alpha}}, \tag{6}$$

where $N = \sum_i N_i$ is the measured $D$ meson yield of the total data sample. The sum in the denominator of Eq. 6 can be rewritten by introducing the average efficiency $\epsilon$, defined by the weighted sum:

$$\epsilon = \sum_i p_i\epsilon_i \quad , \qquad p_i = \frac{A_i^{\alpha}\mathcal{L}_i}{\sum_k A_k^{\alpha}\mathcal{L}_k} \tag{7}$$

Then the expression Eq. 6 reads

$$\Delta\sigma_{\mathrm{pN}} = \frac{N}{\mathrm{Br}\cdot\epsilon\cdot\sum_i \mathcal{L}_i A_i^{\alpha}} \tag{8}$$

Since there is no experimental indication for nuclear effects in open charm production, a linear A dependence of the production cross sections assumed, and $\alpha$ was set to $\alpha = 1$ in Eq. 7 and Eq. 8. This assumption is also in agreement with our measurements as discussed in Section 5.5.

The total systematic uncertainties are, according to Eq. 8, composed of contributions from uncertainty in the signal yields associated with the fitting procedure (listed as 'event fitting'), branching fractions, integrated luminosity and reconstruction efficiency. Furthermore, the uncertainty of the reconstruction efficiency can be divided into contributions from Monte Carlo statistics, track reconstruction efficiency, particle identification efficiency, selection criteria and the contribution from the reweighting of kinematical distributions. The individual contributions are summarized in Table 4 and Table 5. The uncertainty due to selection criteria was determined in two ways, by varying the cut values in the selection criteria discussed above, and by performing a second analysis with an independent set of selection criteria.

The resulting cross sections in the visible range, $\Delta\sigma_{\mathrm{pN}}$ and $\Delta\sigma_{\mathrm{pA}}$, are summarized in tables 6-8. In order to extrapolate the measurements to the full phase space,

$$\sigma_{\mathrm{pN}} = \frac{\Delta\sigma_{\mathrm{pN}}}{f_{\mathrm{vis}}}, \tag{9}$$

the fraction $f_{\mathrm{vis}}$ of $D$ mesons in the visible range defined by $-0.15 < x_{\mathrm{F}} < 0.05$ was determined. With the measured value of the exponent $n = 7.7 \pm 1.4$ as measured by

**Table 5.** Summary of systematic uncertainties of visible cross sections

| Source | $D^0$ | $D^+$ | $D_s^+$ | $D^{*+}$ |
|---|---|---|---|---|
| Event fitting | 3.4% | 2.6% | 6.0% | 9.7% |
| Branching fractions | 1.8% | 3.6% | 13.0% | 1.9% |
| Luminosity | 3.4% | 3.4% | 3.4% | 3.4% |
| Efficiency | 8.4% | 10.3% | 12.9% | 9.7% |
| Total | 10% | 12% | 20% | 14% |

the E743 and E653 experiments [6,7], $f_{\mathrm{vis}}$ was calculated by using the expression Eq. 2. The values corresponding to the choice $x_{\mathrm{b}} = 0.062$ and $x_{\mathrm{b}} = 0$ are $0.542\pm0.048$ and $0.558\pm0.051$, respectively. The difference is small compared to the uncertainty due to the error of parameter $n$. For the extrapolation the average of both numbers, $f_{\mathrm{vis}} = 0.55 \pm 0.05$, was used. The resulting cross sections extrapolated to the full phase space are listed in Table 6.

Figure 5 shows the comparisons of the measured cross sections with other experimental studies. To compare the measurements at different center-of-mass energies, the data points including the results of the present measurement were fitted with theoretical predictions based on different parton distribution functions [1]. In each fit only the normalization parameter was left free while the shape was fixed. Our results provide the most accurate measurement at high energies, and are consistent with previous studies.

The measured sum of the $D$ meson cross sections per nucleon $\sigma(D^0)+\sigma(D^+)+\sigma(D_s^+) = (87.4\pm8.2\pm12.6)$ $\mu$b is used to determine the charm production cross section. From the fractions of charm hadrons produced in the hadronisation of $c$ quarks as measured in $e^+e^-$ collisions, the production of $D^0$, $D^+$ and $D_s$ mesons is found to account for $f_D = 0.891 \pm 0.041$ of the charm cross section [25].

**Table 6.** Cross sections in the visible range ($-0.15 < x_{\mathrm{F}} < 0.05$) and extrapolated to the full phase space. In the second column, the systematic error due to the extrapolation uncertainty is quoted separately.

| | $\Delta\sigma_{\mathrm{pN}}[\mu b]$ (visible range) | $\sigma_{\mathrm{pN}}[\mu b]$ (full $x_{\mathrm{F}}$ range) |
|---|---|---|
| $D^0$ | 26.8±2.6±2.7 | 48.7±4.7±4.9±4.4 |
| $D^+$ | 11.1±1.2±1.3 | 20.2±2.2±2.4±1.8 |
| $D_s^+$ | 10.2±3.5±2.0 | 18.5±6.4±3.7±1.7 |
| $D^{*+}$ | 11.9±2.6±1.7 | 21.6±4.7±3.0±2.0 |

**Table 7.** Cross sections for particle and anti-particle production in the visible range ($-0.15 < x_{\mathrm{F}} < 0.05$).

| | $\Delta\sigma_{\mathrm{pN}}[\mu b]$ | |
|---|---|---|
| | particles | anti-particles |
| $D^0$ | 12.0±1.7±1.2 | 14.8±1.7±1.5 |
| $D^+$ | 4.8±0.8±0.6 | 6.3±0.9±0.8 |
| $D_s^+$ | 4.1±2.3±0.8 | 6.3±2.6±1.3 |
| $D^{*+}$ | 4.5±1.4±0.6 | 7.2±1.5±1.0 |

**Table 8.** Visible cross sections per nucleus. Numbers in parentheses in the last row are for the subsamples of $D^{*+}$ with $D^0$ daughters not common to the $D^0$ samples of the first row.

| | $\Delta\sigma_{\mathrm{pA}}$ [mb] | |
|---|---|---|
| data sample | C | Ti |
| $D^0$ | 0.36± 0.05± 0.04 | 1.01± 0.33± 0.10 |
| $D^+$ | 0.12± 0.02± 0.02 | 0.48± 0.16± 0.06 |
| $D_s^+$ | 0.12± 0.07± 0.02 | 0.15± 0.35± 0.03 |
| $D^{*+}$ | 0.17± 0.05± 0.03 | 0.71± 0.30± 0.10 |
| | (0.21± 0.06± 0.03) | (0.95± 0.50± 0.14) |
| data sample | W | |
| $D^0$ | 4.91± 0.62± 0.54 | |
| $D^+$ | 2.17± 0.32± 0.28 | |
| $D_s^+$ | 2.18± 0.99± 0.46 | |
| $D^{*+}$ | 1.71± 0.51± 0.26 | |
| | (2.11± 0.84± 0.34) | |

Assuming the same fraction, the present study derives the charm cross section per nucleon, $\sigma(c\bar{c}) = (\sigma(D^0) + \sigma(D^+) + \sigma(D_s^+))/(2f_D)$, where the factor 2 accounts for the charge-conjugated states which are included in the $D$ production cross sections. The resulting charm cross section per nucleon as measured in the present study is $\sigma(c\bar{c}) = (49.1 \pm 4.6 \pm 7.4)$ $\mu$b. Note that due to correlations, the systematic error in the sum of cross sections is slightly larger than the value which one would get by adding in quadrature the individual contributions.

## 5.2 Differential cross sections

The differential cross sections $d\sigma/dp_{\mathrm{T}}^2$ and $d\sigma/dx_{\mathrm{F}}$ were determined from production yields in bins of $p_{\mathrm{T}}^2$ and $x_{\mathrm{F}}$ by using the expression Eq. 8. The yield in each individual bin was determined by subtracting from the number of events in the $D$ meson signal window the number of background events as estimated from the sidebands. The resulting differential cross sections for the production of $D^0$ and $D^+$ mesons are shown in Fig. 6.

The parameters of the measured differential cross sections were determined in the following way. Because of the low statistics in individual bins of $p_{\mathrm{T}}^2$ and $x_{\mathrm{F}}$, a direct fit to the data points of Fig. 6 is not adequate. Instead, a simultaneous binned likelihood fit of the $p_{\mathrm{T}}^2$ and $x_{\mathrm{F}}$ distributions for events from the mass signal window and from the sideband windows was performed, by which the Poissonian errors could be treated correctly.

For the transverse momentum distribution, several parametrisations have been found in the literature [2,27,30]. The parametrisation given in expression Eq. 1 was used, and the values of parameters $\langle p_{\mathrm{T}}\rangle$ and $\beta$ were extracted from a fit to the data. The distribution of background events $N_{\mathrm{bgr}}(p_{\mathrm{T}}^2)$ was assumed to be the same in shape and normalization for the signal window and sidebands. Several parameterizations were fitted first to the distributions of the events from sidebands. As many of them fit

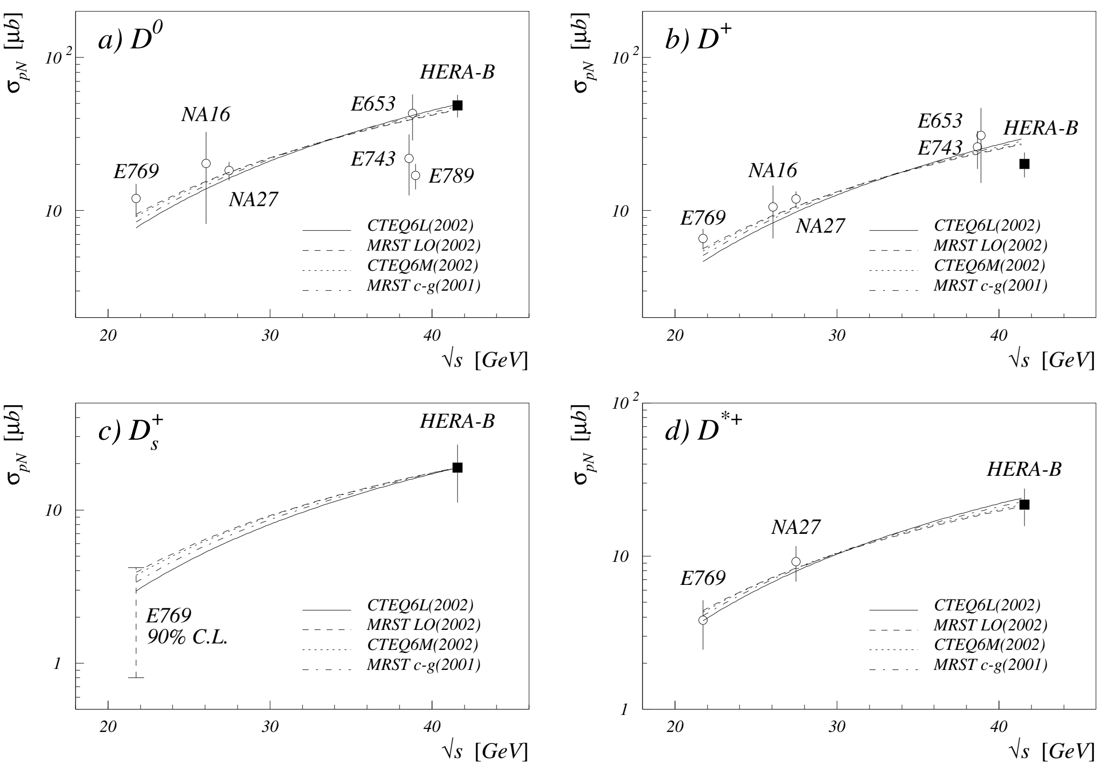


**Fig. 5.** Measured cross sections, and comparison of the results with previous measurements. In figure a) the result of E789 was excluded from the fit. The different curves correspond to different assumptions on parton distribution functions [1].

well, the one among those with two free parameters was chosen which gave the smallest $\chi^2$/ndf: $e^{A+Bp_T^2}$ for $D^0$ and $D^+$, and the same parametrisation multiplied with the efficiency in $p_T^2$, $e^{A+Bp_T^2}\epsilon(p_T^2)$, for $D^{*+}$.

The $D^0$, $D^+$ and $D^{*+}$ data samples were fitted simultaneously, where in the $D^{*+}$ case only a subsample was considered with the $D^0$ daughters not common to the $D^0$ sample. The resulting fit parameters are $\langle p_T \rangle = (1.04 \pm 0.04)$ GeV/$c$ and $\beta = 7.0 \pm 4.3$, with $\chi^2$/ndf=0.86. The measured $\langle p_T \rangle$ is significantly larger (by $3.3\sigma$) than the value extracted from the Pythia Monte Carlo samples (0.90 GeV/$c$), while $\beta$ is within one standard deviation equal to the value extracted from the simulation ($\beta = 4.80$). The fitting was repeated with the fixed value of $\beta = 6$, the same value that was also used for our study of $J/\psi$ production [13]. In this case, the fit yield the same value, $\langle p_T \rangle = (1.04 \pm 0.04)$ GeV/$c$, for $\langle p_T \rangle$, with $\chi^2$/ndf=0.86.

The $x_F$ distribution is usually parameterized with a power-law function:

$$\frac{d\sigma}{dx_F} \propto (1 - |x_F|)^n \tag{10}$$

This function differs in the central region from the predictions of the next-to-leading order QCD calculations [3]. The experimental observation made by E791 [27] in 500 GeV $\pi$-A collisions using a high statistics sample of 80k reconstructed $D^0$ mesons also shows a similar discrepancy. They obtained an improved fit with the function given in Eq. 2, which uses a power-law function in the tail region and a Gaussian in the central region (to account for the asymmetry in $\pi$-A collisions, E791 used an additional offset parameter).

In our analysis of the measured differential cross section $d\sigma/dx_F$ (Fig. 6(b)), the boundary parameter $x_b$ was fixed to the value $x_b = 0.062$ as measured by E791 [27], because our range of $-0.15 < x_F < 0.05$ is too small to be sensitive to this parameter. To extract the exponent $n$, the $D^0$ and $D^+$ data samples were simultaneously fitted with a likelihood fit to the events in the signal windows and sidebands. While the fitted value of the exponent $n = 7.5 \pm 3.2$ agrees with the results of E653 [7] and E743 [6], the error in our study is much larger.

### 5.3 Cross section ratios

The measured cross section ratios are summarized in Table 9. The systematic errors mainly come from selection criteria, event fitting, branching fraction uncertainties and reweighting, while the error in luminosity cancels. The value for the ratio $\sigma(D^+)/\sigma(D^0) = 0.41 \pm 0.06 \pm 0.04$ is the most accurate measurement of this ratio in $pA$ reactions. It is in good agreement with the combined results from hadroproduction [1] as well as from $e^+e^-$ experiments [25]. The ratio also agrees with the latest predictions of Pythia [1], and with a simple prediction based on

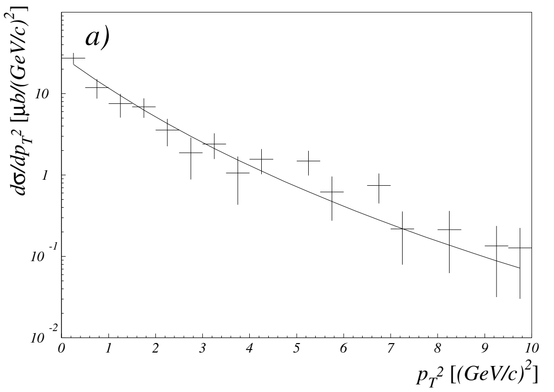


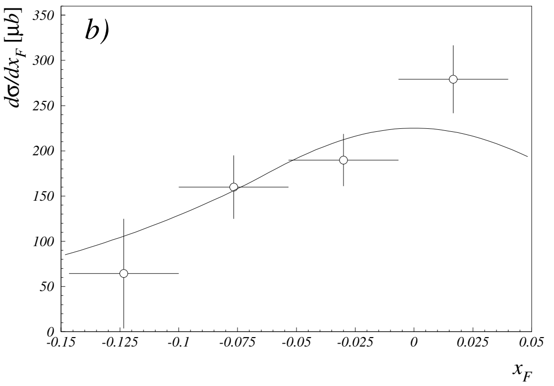


**Fig. 6.** Differential visible cross sections ($-0.15 < x_{\mathrm{F}} < 0.05$) for $D^0$ and $D^+$ production: (a) $d\sigma/dp_{\mathrm{T}}^2$, with the fit of expression Eq. 1, and (b) $d\sigma/dx_{\mathrm{F}}$ with a fit of function Eq. 2 with a free parameter $n$ and a fixed boundary parameter $x_{\mathrm{b}} = 0.062$.

the isospin symmetry and on the measured ratio of vector to scalar meson production cross sections [2].

A comparison with results from other experimental studies is presented in Fig. 7. The ratio $\sigma(D^{*+})/\sigma(D^0) = 0.44 \pm 0.11 \pm 0.05$ is again the most precise measurement of this ratio in $pA$ reactions, and in good agreement with the results of E769 and NA27 [5,9]. The vector to scalar meson production ratio $P_{\mathrm{V}}$ can be calculated in several ways ([1] and references therein) if isospin invariance is assumed. From the ratio $R_1 = \sigma(D^+)/\sigma(D^0)$ one gets $P_{\mathrm{V}} = (1 - R_1)/(1 + R_1)/\mathrm{Br}(D^{*+} \to D^0\pi^+) = 0.61 \pm 0.09 \pm 0.06$, and from $R_2 = \sigma(D^{*+})/\sigma(D^+)$ the value $P_{\mathrm{V}} = R_2/(1+\mathrm{Br}(D^{*+} \to D^0\pi^+)\cdot R_2) = 0.62 \pm 0.09 \pm 0.05$. The results are in good agreement with the world average value $P_{\mathrm{V}} = 0.59 \pm 0.01$ [1].

Our result for the ratio $\sigma(D_s^+)/(\sigma(D^0) + \sigma(D^+)) = 0.27 \pm 0.09 \pm 0.05$ is the first measurement of this quantity in $pA$ reactions. It marginally agrees (within $1.5\sigma$) with the world average value of 0.10±0.02 of measurements in $e^+e^-$ collisions [25].

### 5.4 Leading to non-leading particle asymmetries

The leading particle is defined as the one which has a light quark in common with the beam particle. Thus the leading particles are anti-$D$ mesons $\overline{D}^0$, $D^-$ and $D^{*-}$. The leading to non-leading particle asymmetry is defined as $(\sigma_{LP} - \sigma_{nonLP})/(\sigma_{LP} + \sigma_{nonLP})$. The measured values of the asymmetry in the visible range, $-0.15 < x_{\mathrm{F}} < 0.05$, are given in Table 10 for the $D^0$, $D^+$ and $D^{*+}$ mesons, where the first error is statistical and the second systematic. The latter is dominated by the uncertainty of selection criteria and the kinematical reweighting in respect to possible differences between leading and non-leading particles. Our measurements are consistent with existing measurements of this asymmetry by E769 (0.06±0.06, 0.18±0.05 and 0.36±0.13 for $D^0$, $D^+$ and $D^{*+}$ mesons with $x_{\mathrm{F}} > 0.0$ [9]) and E789 (0.02±0.06 for $D^0$ mesons with $0.0 < x_{\mathrm{F}} < 0.08$ [8]).

**Table 9.** Cross section ratios

| $D^+/D^0$ | $D^{*+}/D^0$ |
|---|---|
| 0.41±0.06±0.04 | 0.44±0.11±0.05 |

| $D_s^+/(D^+ + D^0)$ | $D^{*+}/D^+$ |
|---|---|
| 0.27±0.09±0.05 | 1.07±0.26±0.14 |

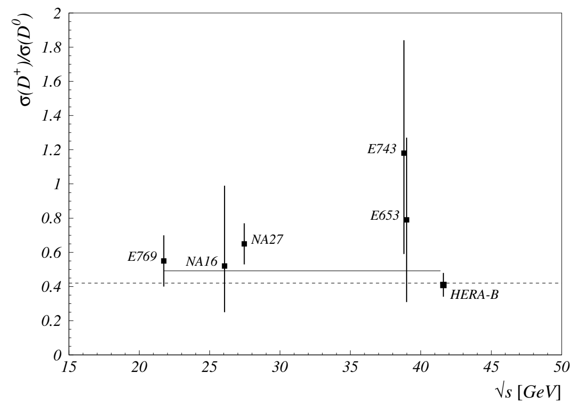


**Fig. 7.** Cross section ratio $R = \sigma(D^+)/\sigma(D^0)$, comparison with previous experiments. The dashed line at $R = 0.42$ shows the prediction based on isospin symmetry with $P_{\mathrm{V}} = 0.6$; the solid line is a fit to the data points.

**Table 10.** Leading to non-leading particle asymmetries in the visible range, $-0.15 < x_{\mathrm{F}} < 0.05$

| $D^0$ | $D^+$ | $D^{*+}$ |
|---|---|---|
| 0.10±0.09±0.05 | 0.14±0.11±0.06 | 0.23±0.17±0.06 |

### 5.5 Atomic mass number dependence

From the measured $D$ meson production on three different target materials (Table 8), the exponent $\alpha$ of the relation Eq. 4 can be determined. The results of simultaneous maximum likelihood fits to the invariant mass distributions of individual material data samples for each $D$ meson are summarized in Table 11. The systematic error comes from

**Table 11.** Atomic number dependency parameter $\alpha$ and a weighted average for the four $D$ mesons. For the weighted average the value in parenthesis of the fifth row were used, corresponding to the subsample of $D^{*+}$ with $D^0$ daughter not common with the $D^0$ sample.

| Particle | $\alpha$ |
|---|---|
| $D^0$ | 0.969±0.057±0.026 |
| $D^+$ | 1.051±0.082±0.028 |
| $D_s^+$ | 1.190±0.402±0.046 |
| $D^{*+}$ | 0.832±0.138±0.022 |
| | (0.847±0.185±0.022) |
| Average | 0.994±0.044±0.025 |

two contributions, uncertainty in the luminosity per wire material (about 2.5%) and Monte Carlo statistics (about 1%). The observed value, $\alpha = 0.99 \pm 0.04 \pm 0.03$, is compatible with a linear dependence of cross sections ($\alpha = 1$). Note that for the weighted average of $\alpha$ over all four samples, only those $D^{*+}$ events were considered for which the $D^0$ daughter particle was not reconstructed in the $D^0$ sample. Our result is in agreement with the result of E789 [8], $\alpha = 1.02 \pm 0.03 \pm 0.02$.

## 6 Summary

With the HERA-B detector we have measured the total and single differential cross sections $\sigma$, $d\sigma/dp_{\mathrm{T}}^2$ and $d\sigma/dx_{\mathrm{F}}$, the atomic number dependence of the cross sections, and the leading to non-leading particle asymmetries for the production of $D^0, D^+, D_s^+$ and $D^{*+}$ mesons in $pA$ collisions at the proton energy of 920 GeV.

Extrapolating to the full phase space, the total cross sections per nucleon (in $\mu$b) were measure: 48.7±4.7±6.6, 20.2±2.2±3.0, 18.5±6.4±4.1 and 21.6±4.7±3.6 for the $D^0$, $D^+$, $D_s^+$ and $D^{*+}$, respectively. In the range $-0.15 < x_{\mathrm{F}} < 0.05$ the measured cross section are: 26.8±2.6±2.7, 11.1±1.2±1.3, 10.2±3.5±2.0 and 11.9±2.6±1.7 for the $D^0$, $D^+$, $D_s^+$ and $D^{*+}$, respectively. The cross section per nucleon for $c\bar{c}$ production is $\sigma(c\bar{c}) = (49.1 \pm 4.6 \pm 7.4)$ $\mu$b.

We have measured the cross section ratios $\sigma(D^+)/\sigma(D^0) = 0.41\pm0.06\pm0.04$ and $\sigma(D^{*+})/\sigma(D^0) = 0.44\pm0.11\pm0.05$, as well as the vector to scalar meson production ratio in two ways, $P_{\mathrm{V}} = 0.62 \pm 0.09 \pm 0.05$ (from $\sigma(D^{*+})/\sigma(D^+)$), and $P_{\mathrm{V}} = 0.61 \pm 0.09 \pm 0.06$ (from $\sigma(D^+)/\sigma(D^0)$). Our result for the ratio $\sigma(D_s^+)/(\sigma(D^0) + \sigma(D^+)) = 0.27 \pm 0.09 \pm 0.05$ is the first measurement of this quantity in $pA$ reactions, and is in marginal agreement with measurements from $e^+e^-$ collisions.

From the measured atomic number dependence of the production cross section, the parameter $\alpha = 0.99 \pm 0.04 \pm 0.03$ is extracted. This value is in agreement with the assumption of a linear dependence of cross sections, $\alpha$=1. The measured leading to non-leading particle asymmetries in the $x_{\mathrm{F}}$ range $-0.15 < x_{\mathrm{F}} < 0.05$ are consistent with existing measurements for different $x_{\mathrm{F}}$ regions.

The results of our studies are in good agreement with previous measurements and provide in most cases the most accurate measurements in $pA$ interactions.

## Aknowledgments

We express our gratitude to the DESY laboratory for the strong support in setting up and running the HERA-B experiment. We are also indebted to the DESY accelerator group for their continuous efforts to provide good and stable beam conditions. The HERA-B experiment would not have been possible without the enormous effort and commitment of our technical and administrative staff. It is a pleasure to thank all of them.

## References

1. C. Lourenço, H. Wöhri, *Phys. Rept.* **433**, (2006) 127.
2. S. Frixione, M.L. Mangano, P. Nason, G. Ridolfi G, *Adv.Ser.Direct High energy Phys.* **15**, (1998) 609.
3. P. Nason, S. Dawson, R.K. Ellis *Nucl. Phys.* **B327**, (1989) 49.
4. M. Aguilar-Benitez *et al* (NA16 Collaboration) *Phys. Lett.* B **135**, (1984) 237.
5. M. Aguilar-Benitez *et al* (NA27 Collaboration) *Z. Phys.* C **40**, (1988) 321.
6. R. Ammar *et al* (E743 Collaboration) *Phys. Rev. Lett.* **61**, (1988) 2185.
7. K. Kodama *et al* (E653 Collaboration) *Phys. Lett.* B **263**, (1991) 573.
8. M.J. Leitch *et al* (E789 Collaboration) *Phys. Rev. Lett.* **72**, (1994) 2542.
9. G.A. Alves *et al* (E769 Collaboration) *Phys. Rev. Lett.* **77**, (1996) 2388. (Erratum-ibid. 1998 **81** 1537)
10. M. Cacciari, P. Nason P, R. Vogt, *Phys. Rev. Lett.* **95**, (2005) 122001.
11. I. Abt (HERA-B Collaboration) *et al Phys. Rev.* D **73**, (2006) 052005.
12. I. Abt (HERA-B Collaboration) *et al Phys. Lett.* B **638**, (2006) 13.
13. I. Abt (HERA-B Collaboration) *et al Phys. Lett.* B **638**, (2006) 407.
14. I. Abt (HERA-B Collaboration) *et al* 2007 *Eur. J. Phys.* C **49**, (2006) 545.
15. K. Ehret *et al Nucl. Instrum. Methods* A **446**, (2000) 190.
16. C. Bauer *et al Nucl. Instrum. Methods* A **501**, (2003) 39.
17. W. Gradl *et al Nucl. Instrum. Methods* A **461**, (2001) 80.
18. H. Albrecht *et al Nucl. Instrum. Methods* A **541**, (2005) 610.
19. H. Albrecht *et al Nucl. Instrum. Methods* A **576**, (2007) 313.
20. I. Ariño I *et al Nucl. Instrum. Methods* A **516**, (2004) 445.
21. G. Avoni *et al Nucl. Instrum. Methods* A **461**, (2001) 332.
22. V. Eiges *et al Nucl. Instrum. Methods* A **461**, (2001) 104.
23. R. Battiston R *et al Nucl. Instrum. Methods* A **238**, (1985) 35.
24. M. Bruschi *et al* arXiv:0706.0131 [hep-ex] (2007)
25. W.M. Yao *et al* (Particle Data Group) *J. Phys. G: Nucl. Part. Phys.* **33**, (2006) 1.
26. T. Sjostrand Comp. Phys. Commun. **82**, (1994) 74.

27. E.M. Aitala *et al* (E791 Collaboration) *Phys. Lett.* B **462**, (1999) 225.
28. H. Pi Comp. Phys. Commun. **71**, (1992) 173.
29. R. Brun *et al* *GEANT3* (Internal Report CERN-DD/EE/84-1, CERN) (1987)
30. G.A. Alves *et al* (E769 Collaboration) *Phys. Rev. Lett.* **77**, (1996) 2392.